A Comparative Analysis of Geometric and Image-Based Volumetric and Intensity Data Registration Algorithms

Dana Cobzaş, Hong Zhang and Martin Jägersand
Department of Computing Science
University of Alberta
Edmonton, Alberta, Canada
{dana, zhang, jag}@cs.ualberta.ca

Abstract

We present and contrast four methods for registering 3D range data to 2D images. Two are calibration techniques that recover the rigid transformation between the sensor poses, based on point or line correspondences. The two others recover a direct, image based mapping between the data sets. The accuracy of each method is experimentally evaluated on test patterns and objects. We found the point based calibration method to best recover a global registration between the two sensors, while an image-based method performed best when registering local regions.

1. Introduction

The registration of volumetric and intensity data is an important problem especially in the fields of model building and realistic rendering (registering range and image data) and in medical applications. Note that the problem is eliminated when the data is acquired using the same sensor as in the case of range from stereo, structured light or range and radiance images acquired by a laser rangefinder, but it becomes complex when data come from two or more sensors. In our case we want to register range data provided by a laser rangefinder with an image acquired by a camera near the laser rangefinder (see Figure 1).

The registration is related to the camera calibration [13] and object pose with the difference that in this case the geometry of the calibration object is unknown so correspondence is a nontrivial problem. The mathematical foundation for pose estimation from points, lines and curves has been extensively studied [2, 5]. The solution is in general nonlinear and requires a good initial estimate of the parameters.

In the case of *medical imaging*, different types of data that contain spatial information both anatomical and functional (MRI, CT, X-ray and camera images of the patient) need to be correlated to plan or control the therapy. For registering an MRI data with the current view of the patient, Grimson [4] uses an intermediate laser that provides a 3D description of the patient's surface. This surface is matched with the volumetric data and, by computing the laser-camera displacement, the medical image is fused with the video image. An interesting approach is presented in [3] where 3D-3D and 2D-3D registration are performed using bitangent lines or planes and an Iterative Closet Point algorithm. This method is applied for registering MRI, image and stereo data.

For *modeling and rendering*, 3D or range data acquired by a laser rangefinder has to be registered with the corresponding images. In [6] multiple scans are integrated with intensity data to create a high resolution image-based scene model. In their case the registration problem is simplified by placing the laser and the camera on the same location so that the transformation is reduced to a pure rotation. If the sensors are not aligned a full 3D transformation have to be recovered in order to register the range with intensity data set. A robust solution that uses corresponding line segments is proposed in [9]. Another approach presented by Ikeuchi *et al.* [8] aligns intensity edges with 3D reflectance edge points and estimated the pose using a robust M-estimator algorithm.

Regardless of the application, all the above methods attempt to recover the rigid transformation between the sensors in order to register the data sets. As mentioned previously, this is in general a nonlinear problem and it requires an initial estimate to converge. In contrast, image-based techniques compute a direct mapping between the points in the data sets that recover the transformation under some constraints. The accuracy of this methods depends on the original assumptions about the physical system (ex. affine camera or planar scene) but in general they are good for locally recovering a mapping between data sets as opposed to determine a globally valid translation and rotation between the sensors.

In this paper we describe our study that investigates the performance and applicability of geometric-based techniques and image-based techniques in the problem of laser-camera registration. For evaluating the results we used the determined transformation to register data taken from an object placed in a different position than the original calibration object. The remaining of the paper is organized as follows. Section 2 presents the type of sensors we use and the data acquisition process. Section 3 describes the theoretical aspects of the different calibration algorithms. Experimental results are presented in Section 4, and we conclude with a discussion in Section 5.

2. Data Acquisition and Preprocessing

The data acquisition system consists of a *laser rangefinder* mounted on a *pan-tilt unit* and a *camera* that is placed in the vicinity of the laser (see Figure 1).

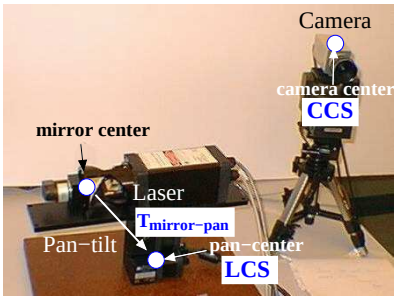

Figure 1: Laser - mirror - camera system. CCS = camera coordinate system; LCS = laser coordinate system

The laser rangefinder is the commercial AccuRange 4000-LIR from Acuity Research, Inc. We attached it to a pan-tilt unit (model PTU-46-70) from Directed Perception, Inc. The data returned for each rangefinder sample consist of range r, amplitude a and encoder position - which can be converted to an angle θ. In addition to these we store the pan angle ϕ at which the scan was taken, so the raw data for each reading is (r, a, ϕ, θ).

The raw data acquired by the laser scanning system is first transformed into 3D points registered into a common coordinate system. The center of the mirror (rotation θ) is translated with respect to the center of the pan-tilt unit (rotation ϕ). We manually measure this displacement and account for it when computing the 3D coordinates of the points. We project these points into a spherical grid and filter the data [6] to produce a spherical amplitude and range image.

If the laser beam clips the edge of one surface and then hits another surface further away, the resulting range is usually between the two surfaces. In order to eliminate the outliers, we look at the eight nearest neighbors on the spherical grid and, if at least four are within a tolerance, the value is considered valid, otherwise it is removed. We also remove all the values that are bigger then the dimension of the room where we did the experiments.

For filling the places that are not scanned well, we apply a 3×3 filter that averages the neighboring samples. Figure 2 shows an example of a spherical range and amplitude image after filtering.

3. Laser-Camera Calibration

Calibrating the laser with respect to the camera involves determining the transformation that will map 3D points in laser coordinate system (LCS) to 2D image points in camera coordinate system (CCS) given a set of corresponding features in the two sensors (see Figure 1). We have developed several methods - *point-based*, *line-based* and two types of *image-based* methods. The first two methods recover the full 3D rigid transformation (R, t) between the two reference coordinate systems, assuming that the camera matrix (C) is known. The last type of methods use image-based techniques to map 3D points to image pixels without considering any calibration data.

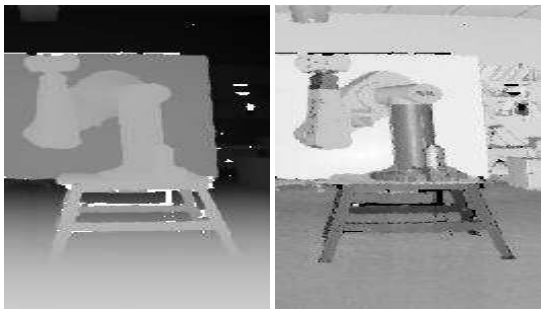

(a) (b)

Figure 2: Spherical range (a) and amplitude (b) images after filtering

The problem is conceptually similar to the camera calibration or more precisely object pose problem, with the key difference that in our case the 3D information about the calibration object acquired by the laser is a collection of range/amplitude values along scan lines and not precise 3D measurements of feature points. As mentioned in Section 2, the laser range-finder returns range and amplitude values of a 360° vertical scan for each position of the pan-tilt unit. The trace of the laser is visible in the camera so, by recording a scan and the light path in the camera image, we can establish corresponding features for each scan plane. The extracted features are intersections of object discontinuities with the laser line. The line-based algorithm and one of the image-based algorithms use these features along the scan lines. Yet, another way to get corresponding features is to relate a range/amplitude image obtained by a full scan (Section 2) and a camera image of the same scene.

3.1. Line Based Algorithms

A 3D line can be represented in terms of a unit vector $\mathbf{v}$, which indicates the direction of the line, and a vector $\mathbf{d}$, which represents a point on the line that is closet to the origin [11] (see Figure 3). The line and the camera center defines a plane whose normal vector is $\mathbf{m}$. Under perspective projection, the image line is determined by the intersection of this plane with the image plane. Assuming unit focal length (normalized image coordinates), the equation of the image line is:

$$m_x x + m_y y + m_z z = 0$$

where $\mathbf{m} = (m_x, m_y, m_z) = \mathbf{v} \times \mathbf{d}$.

We denote by $(\mathbf{v}_l, \mathbf{d}_l)$ the line in laser coordinate system (LCS), $(\mathbf{v}_c, \mathbf{d}_c)$ the line in camera coordinate system (CCS) and $(\mathbf{R}, \mathbf{t})$ the general rigid transformation between CCS and LCS. The projection of the image line in the image plane is:

$$\mathbf{m} = \mathbf{v}_c \times \mathbf{d}_c = \mathbf{R}\mathbf{v}_l \times (\mathbf{R}\mathbf{d}_l + \mathbf{t})$$

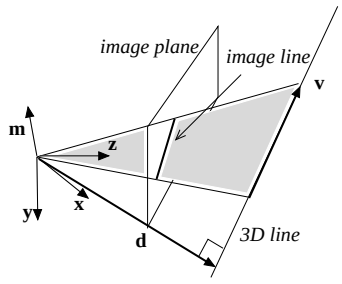

Figure 3: A 3D line can be represented as $(\mathbf{v}, \mathbf{d})$. The image projection is represented by $\mathbf{m}$

From this equation the following constraints can be deduced:

$$\mathbf{m}^T(\mathbf{R}\mathbf{v}_l) = 0, \;\; \mathbf{m}^T(\mathbf{R}\mathbf{d}_l + \mathbf{t}) = 0 \tag{1}$$

The rotation can be represented by a unit quaternion $\mathbf{q}$ with the property that $\mathbf{R}\mathbf{v} = \mathbf{q} * \tilde{\mathbf{v}} * \overline{\mathbf{q}}$, where "*" denotes quaternion multiplication, $\overline{\mathbf{q}}$ is the conjugate quaternion and $\tilde{\mathbf{v}}$ is the imaginary quaternion associated with $\mathbf{v}$. We can rewrite Equation **??** as:

$$\mathbf{m}^T(\mathbf{q} * \mathbf{v}_l * \bar{\mathbf{q}}) = 0, \;\; \mathbf{m}^T(\mathbf{q} * \mathbf{d}_l * \bar{\mathbf{q}} + \mathbf{t}) = 0 \tag{2}$$

Having N corresponding lines we can solve for the rotation $\mathbf{q}$ by minimizing the objective function

$$\begin{array}{l} \mathcal{F}_{LRt} = \sum_{i=1}^{N} (\mathbf{m}_i^T(\mathbf{q} * \mathbf{v}_{li} * \bar{\mathbf{q}}))^2 \\ \left\{ \begin{array}{l} \min_{\mathbf{q}} \mathcal{F}_{LRt} \\ |\mathbf{q}| = 1 \end{array} \right. \end{array} \tag{3}$$

If the rotation is known, the translation $\mathbf{t}$ can then be calculated from Equation 2. For N points we solve it as a linear least square problem. After having an initial estimate for the rigid transformation $(\mathbf{R}, \mathbf{t})$, we refine the solution by globally minimizing the objective function:

$$\begin{array}{l} \mathcal{F}_{LG} = \sum_{i=1}^{N} (\mathbf{m}_i^T(\mathbf{q} * \mathbf{v}_{li} * \bar{\mathbf{q}}))^2 + (\mathbf{m}_i^T(\mathbf{q} * \mathbf{d}_{li} * \bar{\mathbf{q}} + \mathbf{t}))^2 \\ \left\{ \begin{array}{l} \min_{\mathbf{q}} \mathcal{F}_{LG} \\ |\mathbf{q}| = 1 \end{array} \right. \end{array} \tag{4}$$

We solve the non-linear minimization problems using a Levenberg-Marquardt non-linear minimization algorithm [7]. The problem has a unique solution with at least four corresponding lines where no more than two lines intersect in the same point (or are parallel). In our experiments the rotation is mostly a pan so, for having an initial estimate for the rotation, we linearly solve Equation 1 with the rotation matrix constrained to a pan.

3.2. Point Based Algorithms

The point based algorithm is similar to the line based algorithm. Let $\mathbf{p} = (x, y, 1)$ represent the normalized homogeneous coordinates of an image pixel (u, v),

$$x = \frac{u - u_c}{\alpha_u}, y = \frac{v - v_c}{\alpha_v}$$

where α_u and α_v are the vertical and horizontal scale factors and u_c and v_c are the pixel coordinates of the center of the image, all assumed to be known. If $\mathbf{P}_l$ is the corresponding 3D point in LCS we have:

$$s\mathbf{p} = \mathbf{R}\mathbf{P}_l + \mathbf{t}$$

Having more than six corresponding points ($N > 6$), we first solve the problem linearly without any constraints on the rotation matrix and then refine the solution by minimizing the distance between the projected image points and the corresponding extracted features

$$\mathcal{F}_{PN} = \sum_{i=1}^{N} \sqrt{(u_i - u_{il})^2 + (v_i - v_{il})^2}$$

where $\mathbf{p}_l = (x_l, y_l, s_l) = \mathbf{R}\mathbf{P}_l + \mathbf{t}$ and $u_l = \frac{x_l}{s_l}$, $v_l = \frac{y_l}{s_l}$. As in the case of line features, we solve the nonlinear problem using a Levenberg-Marquatdt non-linear minimization algorithm. The linear solution is very unstable and sensitive to errors in the extracted features so in the experiments we solve the linear problem by constraining the rotation to a pan.

3.3. Affine camera approximation

Image based techniques do not rely on any precise calibration measurements like camera matrix or rigid transformation but compute the transformation that maps pixels directly from image space to the desired space. They are mostly used in image-based rendering when pixels from sample images are mapped to new locations in the rendered images without recovering the 3D Euclidean structure of the scene. In the case of laser-camera calibration, the proposed image-based techniques will recover a direct transformation from the laser points to image pixels.

Following [12], let (u_i, v_i) be the set of extracted image pixels and $m = (m_u, m_v)$, $m_u = \frac{1}{N}\sum_{i=0}^{N} u_i$, $m_v = \frac{1}{N}\sum_{i=0}^{N} v_i$ be their centroid. Compose measurement matrices

$$W = \begin{pmatrix} \mathbf{u} \\ \mathbf{v} \end{pmatrix} \; \bar{W} = \begin{pmatrix} \mathbf{u} - m_u \\ \mathbf{v} - m_u \end{pmatrix}$$

where $\bar{W}$ is zero mean and is called the *registered measurement matrix*.

Rank theorem Under orthography $rank(\bar{W}) = 3$ (for proof see [12]). Under most viewing conditions with a real camera the effective rank is 3. The registered measurement matrix $\bar{W}$ can be expressed as

$$\bar{W} = RS$$

where $S = (P_1 \; ... \; P_N)$ is the shape matrix with the affine coordinates of $(u_1; v_1) \; ... \; (u_N, v_N)$ and $R = \begin{pmatrix} \mathbf{I} \\ \mathbf{J} \end{pmatrix}$ represents the camera rotation. In fact, the rows of R can be interpreted as the orientation of the vertical and horizontal image axes in the range data and the columns as the projections of the affine basis vectors into the image. Hence rotation and

scaling are represented by R and image plane translation by $\mathbf{m} = (m_u, m_v)$. The columns of S are 3D affine coordinates of the feature points with respect to their centroid. In our case, S is formed with the 3D coordinates of the laser points (normalized with respect to centroid m_P) and W with the corresponding image features.

Reprojection property Given a new set of 3D points P' in the laser coordinate system they can be reprojected by

$$\begin{pmatrix} u' \\ v' \end{pmatrix} = R(P' - m_P) + \begin{pmatrix} m_u \\ m_v \end{pmatrix}$$

The laser-camera transformation can be represented by the rotation matrix R, the centroid of image test points m and the centroid of the corresponding laser points $m_P = (X_0, Y_0, Z_0)$.

Compared to the projective model $u = f\frac{X}{Z} + u_c$ this approach is approximating the $\frac{1}{Z}$ variation in depth with a line $u = s(X - X_0) + k(Z - Z_0)$. As a consequence we expect that the algorithm will work for objects that have a small range variation.

3.4. Plane homography

Another image-based technique can be derived by considering the laser scan plane and its image projection. It is well known [10] that planar scene views are related by 2D projective transformations (homographies).

$$\mathbf{u} = \mathbf{H}\mathbf{p}$$

This transformation is up to a scale so in general $\mathbf{H}$ has eight independent parameters.

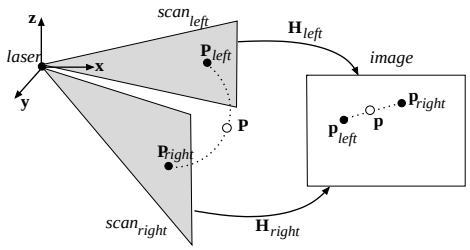

Figure 4: Mapping points using the homographies of the closest laser scan planes

Laser points in each scan are on a vertical plane. When panning the laser it generates planar points for each scan. These points are related to their image projection by a homography $\mathbf{H}_i, i = 1, ..., M$, where M is the number of sampled scan planes. The homography for each scan plane can be computed from at least 4 corresponding points. Knowing the homography $\mathbf{H}_i$, 3D laser points that lie on the same plane can be reprojected on the image plane. For a point $\mathbf{p}$ that lies in between the originally sampled scan planes, we compute its projection as the interpolation between the projection of this point through the homographies $\mathbf{H}_{left}$ and $\mathbf{H}_{right}$ corresponding to the closet sampled scan planes. More precisely (see Figure 4), if $\mathbf{p}$ is lying on the scan plane at pan angle ϕ and the closest sampled scan planes were taken at ϕ_{left} and ϕ_{right}, the projection of $\mathbf{p}$ is

$$\begin{aligned} \mathbf{u}_{left} &= \mathbf{H}_{left}\mathbf{p} \\ \mathbf{u}_{right} &= \mathbf{H}_{right}\mathbf{p} \\ \bar{\mathbf{u}} &= \tfrac{\phi - \phi_{left}}{\phi_{right} - \phi_{left}}\bar{\mathbf{u}}_{left} + \tfrac{\phi_{right} - \phi}{\phi_{right} - \phi_{left}}\bar{\mathbf{u}}_{right} \end{aligned}$$

where $\bar{\mathbf{u}}$ represents the affine coordinates of the homogenious point $\mathbf{u}$ (divided by the scale factor).

Note that when moving from scan plane $scan_{right}$ to $scan_{left}$ $\mathbf{p}$ describes a circular arc whose projection in the image is an elliptic arc. Following from this the exact projection of $\mathbf{p}$ can be computed as the interpolation along this ellipse of $\mathbf{p}_{left}$ and $\mathbf{p}_{right}$. This can be done if we know the projection of $\mathbf{p}$ in four or more scan planes. In the approach we took we approximate the elliptic arc with a straight line. For small rotations this is a reasonable approximation.

4. Experimental Results

4.1. Feature extraction

The proposed calibration algorithms require corresponding point and line features. There are two different approaches for extracting corresponding features. One is to extract and match features that are distinctive in both camera image and range/amplitude spherical laser images. The other method relies on the property that the laser scan-line is visible in the camera image, so that features along each scan line can be put in correspondence with image pixels if there is an image taken at the scan time.

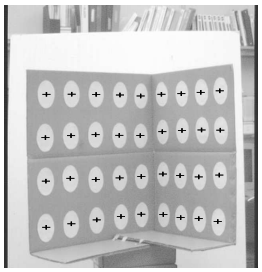

Figure 5: Image of the calibration pattern and the corresponding laser amplitude image. The extracted feature points are marked with '+'

For the first method we design a calibration pattern similar to the one usually used for camera calibration with white dots on two planes. We threshold both the camera and laser amplitude images, and then extract centroids of the black dots (see Figure 5). The point extraction and correspondence process is semi-automatic. In order to have a significant variation in depth, we repeat the process for images in four positions one in front (`pattern 1`) and three further back (`pattern 2,3,4`) extracting about 150 corresponding points. The point based (**PL**,**PN**) and the first type of image based algorithm (**IA**) are using this type of data.

For the second method we placed boxes at different depths in front of the laser-camera system and record six scans and the corresponding camera images (`boxes 1-6`)

Algorithm	*Calibration features*	*Feature extraction alg.*	*Calib method*
LRT	image-3D lines	range and images of scan planes	first estimates rot. **R** and then transl. **t**
LG	image-3D lines	range and images of scan planes	globally minimize both **R** and **t**
PL	image-3D points	calibration pattern	linear solution for both **R** (pan) and **t**
PN	image-3D points	calibration pattern	globally minimize both **R** and **t**
IA	image-3D points	calibration pattern	affine approximation of camera
IH	image points - 2D points on scan planes and pan angle	range and images of scan planes	interpolation of scan planes' homographies

Table 1: Summary of calibration algorithms

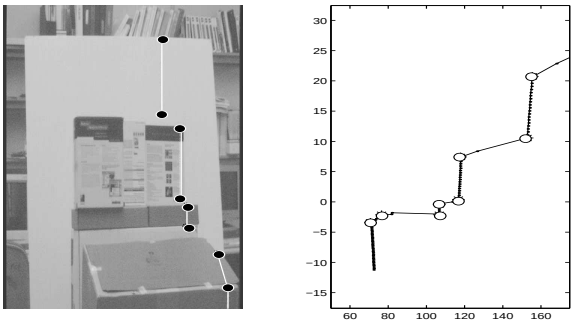

Figure 6: Image of a scan line and corresponding laser points. Corresponding feature points are marked with a circle.

(see Figure 6). We designed an user interface that allows the selection of corresponding points along the scan. For the line based algorithm the user extracts corresponding lines by selecting two points along each line. In general there are about 6 to 8 corresponding points and 4 or 5 lines.

4.2. Point reprojection error

For testing the accuracy of the calibration algorithms we compute the error between the reprojected 3D point features and the corresponding image features. Table 1 presents a summary of the implemented calibration algorithms.

Alg	*Calibration data*	*Error*
LRT	`boxes 1-6`	34.85
LG	`boxes 1-6`	26.25
PL	`patterns 1-4`	62.16
PN	`patterns 1-4`	15.63
IA	`patterns 1-4` (range variation)	19.46
	`patterns 2,4` (similar range)	4.66
IH	`boxes 1-6`	25.51

Table 2: Average pixel/feature error between projected points and extracted features for different algorithms

We took a full scan of the calibration pattern in a new position (`pattern 5`), different from the ones used for calibration, together with an image of the pattern, and we apply the point extraction algorithm. Table 2 summarizes the performance of different types of algorithms on this data set.

For testing the influence of the errors present in the calibration data on geometric and image-based algorithms, we projected this data back to the original images. The pixel/feature error is about 5 pixels for the image-based techniques and about 15 pixels for point based techniques. This shows that the image-based techniques are more flexible to data fitting and local inaccuracies of the model than the geometric-based approaches, which impose a rigid transformation. From this we can also expect that the image feature extraction error is within the range 5 to 15 pixels.

4.3. Applications

The registered image-range data can be used to rerender an object from a different position than the original image. We used the data from the scanned robot arm. The object data is first segmented from the background (threshold range values) and the remaining points are projected on the image. We triangulate the image points using a 2D Delaunay triangulation and render the corresponding 3D triangles using OpenGL. In a complete mesh, some of the triangles might not represent physical planes, and in most of the cases this appears at silhouette edges [6] where points from the object are connected with background points. To avoid this phenomenon we eliminate all the triangles that are parallel to the viewing direction within a threshold. The results for the rendered arm with the four registration algorithms are presented in Figure 7.

The image-based rendering idea can be applied to the problem of mobile robot localization. We have created a panoramic image-based model of the navigation environment [1]. The model is a panoramic mosaic formed from images taken by rotating the camera around the optical center. This model can be registered with the laser range data in a similar way we registered the planar image. The localization problem involves finding the position and orientation of the robot using the image-based model and assuming that the robot is carrying an on-board camera. The registered intensity-range data is used to generate new renderings from any location. The position of the robot can be computed from the displacement between the actual image taken by the robot and a rendered image from the vicinity of the robot (assuming the approximate location is known - from odometry for example).

5. Discussion and Conclusion

We have presented four 2D-3D registration algorithms addressing the problem of registering range data acquired from

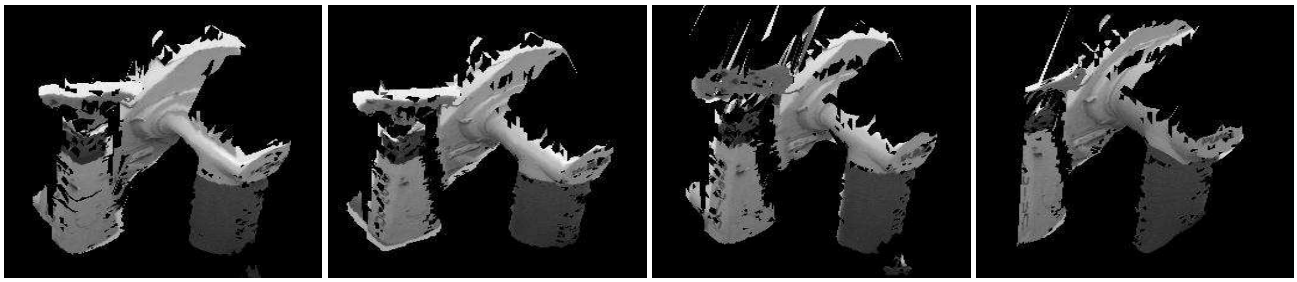

(a) (b) (c) (d)

Figure 7: Rendered arm images with different registration algorithms (a) point based (b) line based (c) affine camera approximation (d) scan planes' homographies

a laser rangefinder and intensity data from a camera near the laser. Two of the algorithms (point-based **PL**, **PN** and line-based **LRT** and **LG**) are recovering the rigid 3D transformation between the sensors (rotation $\mathbf{R}$ and translation $\mathbf{t}$) and the other two (**IA** and **IH**) are computing a local mapping between range points and image pixels.

The nonlinear versions (**PN** and **LG**) of the geometry-based algorithm are performing better when applied to a data set different than the calibration data (*e.g.* robotic arm scan, Figure 7). The linear image-based algorithm (**IA**) is very good when there is little range variation in the 3D data. This is because it uses an affine camera model, which allow a somewhat more general fit of the data than the rigid transformation in point and line based algorithms. The homography based algorithm (**IH**) correctly models the perspective 3D-2D transformation for each of the scan planes. Its performance can be improved if more scan planes are considered in the calibration process, but this will require an automatic feature detection and matching algorithm. Its main drawback is that several features have to be found in each scan plane.

In general, the applicability of each of the presented methods is dependent on the practical problem that has to be solved. The geometric-based methods are more suitable in applications that require high precision - like medical imaging applications. A line-based method will work better if line/edges are presented in the data set (*e.g.* modeling an office type environments). When the camera has high distortion and it can not be modeled as a perfect projective camera, the image based algorithms can be applied to locally recover the transformation for portions of the data set. The image-based methods are in general fast and can be used for applications that require real-time registration like in robotics.

In the future, we will apply the registration algorithms to a panoramic image and the laser range scan to create an image-based model for robot navigation. In this problem we have to model a more complicated cylindrical projection for the image data.

References

[1] D. Cobzas and H. Zhang. Cylindrical panoramic image-based model for robot localization. In *Proc. of IROS*, Hawaii, October 2001.

[2] O. D. Faugeras. *Three Dimensional Computer Vision: A Geometric Viewpoint*. MIT Press, Boston, 1993.

[3] J. Feldmar, N. Ayache, and F. Betting. 3d-2d projective registration of free-form curves and surfaces. *Computer Vision and Image Undestanding*, 65(3):403–424, 1997.

[4] W.E.L. Grimpson, T. Loranzo-Perez, W.M. Wells III, G.J. Ettinger, S.J. White, and R.Kikinis. An automatic registration method for frameless stereotaxy, image guided surgery and enhanced reality visualization. In *Proc of CVPR*, Seattle, June 1994.

[5] R. M. Haralick, H. Joo, C.-N. Lee, X. Zhuang, and M. B. Kim. Point estimation from corresponding point data. *IEEE Trans. Systems, Man Cybernetics*, 19(6), 1989.

[6] D. K. McAllister, L. Nyland, V. Popescu, A. Lastra, and C. McCue. Real-time rendering of real world environments. In *Proc. of Eurographics Workshop on Rendering*, Spain, June 1999.

[7] W. H. Press, B.P. Flannery, S. A. Teukolsky, and W. T. Vetterling. *Numerical Recipies in C: The Art of Scientific Computing*. Cambridge University Press, Cambridge, England, 1992.

[8] M. D. Wheeler R. Kurazume and K. Ikeuchi. Mapping textures on 3d geometric model using reflectance image. In *Proc. of the Data Fusion Workshop in IEEE, ICRA)*, 2001.

[9] I. Stamos and P. K. Allen. 3D model construction using range and image data. In *Proc. of CVPR*, 2000.

[10] R. Szeliski. Video mosaics for virtual environments. *IEEE Computer Graphics and Applications*, pages 22–30, March 1996.

[11] C. Taylor and D. J. Kriegman. Structure and motion from line segments in multiple images. *IEEE Transactions on Pattern Analysis and Machine Intelligence*, November 1995.

[12] C. Tomasi and T. Kanade. Shape and motion from image streams under orthography: A factorization method. *International Journal of Computer Vision*, 9:137–154, 1992.

[13] R. Tsai. A versatile camera calibration technique for high accuracy 3d machine vision metrology using off-the-self tv cameras and lenses. *IEEE Journal of Robotics and Automation*, 3(4):323–344, 1987.